Sensors and Actuators B 268 (2018) 170–181

Contents lists available at ScienceDirect

Sensors and Actuators B: Chemical

journal homepage: www.elsevier.com/locate/snb

Room-temperature, high selectivity and low-ppm-level triethylamine sensor assembled with Au decahedrons-decorated porous α-Fe_2O_3 nanorods directly grown on flat substrate

Xiaopan Song [a], Qi Xu [a], Tao Zhang [b], Bao Song [c], Cuncheng Li [b], Bingqiang Cao [a,d,*]

[a] Materials Research Center for Energy and Photoelectrochemical Conversion, School of Materials Science and Engineering, University of Jinan, Jinan 250022, Shandong, China
[b] School of Chemistry and Chemical Engineering, University of Jinan, Jinan 250022, Shandong, China
[c] School of Mechanical Engineering, University of Jinan, Jinan 250022, Shandong, China
[d] School of Physics and Physical Engineering, Qufu Normal University, Qufu 273165, Shandong, China

ARTICLE INFO

Article history:
Received 5 January 2018
Received in revised form 18 April 2018
Accepted 19 April 2018
Available online 22 April 2018

Keywords:
Au/α-Fe2O3 nanorods
Porous materials
TEA sensor
Near room-temperature
Schottky contact

ABSTRACT

Chemiresistive based gas sensors with low operating temperature (e.g. room-temperature), high selectivity, and fast response for specific target gas are highly desired. Herein, we successfully construct triethylamine (TEA) gas sensors with gold (Au) decahedrons (DHs)-decorated porous α-Fe_2O_3 nanorods, which can work at 40 °C and exhibit high selectivity and low-ppm-level response. Porous α-Fe_2O_3 nanorods with high specific surface area are directly grown on seeded flat substrate with electrodes by a cost-effective hydrothermal method. Au DHs synthesized by one-pot polyol reaction method are deposited onto such α-Fe_2O_3 nanorods by spin-coating. Such Au DHs/α-Fe_2O_3 nanorods sensor working at temperature as low as 40 °C and relative humidity (RH) of 30% exhibits high response (17–50 ppm TEA), low detection concentration (~1 ppm), and short response/recovery time (12/8 s), which are all much better than the control α-Fe_2O_3 nanorods sensor. When the RH increases, the sensor response decreases due to the water molecules adsorption. Furthermore, the enhanced sensing properties toward TEA are discussed in terms of the formation of Au/Fe_2O_3 metal/semiconductor Schottky contact and the catalytic activity of Au DHs.

1. Introduction

Triethylamine (TEA) gas sensors have drawn much attention for wide application in chemical industry. TEA is explosive and can cause irritations to the dermal, ocular, and respiratory systems if the concentration is higher than 10 ppm in air [1,2]. In addition, long-term exposure to TEA may eventually result in abnormal embryos [3–5]. Traditional methods such as gas/liquid/film chromatography and electrochemistry analysis have been adopted to detect TEA gas [6,7]. However, their further applications are limited because of the complex operation, expensive apparatus cost, and strict testing environment. Therefore, it is still a strong demand to develop convenient, fast, and portable instrument with high selectivity and sensitivity to detect TEA gas in daily life or industrial production process [8].

Metal oxide semiconductor (MOS) nanostructures such as ZnO [9], SnO_2 [10], In_2O_3 [11], and α-Fe_2O_3 [12–15] have been widely adopted as gas sensing materials with some advantages like simple growth and fast response. Among them, hematite (α-Fe_2O_3), as a typical *n*-type transition MOS with a band gap of 2.1 eV [16] has exhibited impressive sensing property to acetone [17], toluene [18], ethanol [19], formaldehyde [20], and so on. Nevertheless, gas sensors for TEA detection based on α-Fe_2O_3 have been reported very little. Sun et al. [21] fabricated mesoporous α-Fe_2O_3 microrods for TEA gas sensors, which showed a response of 11.8–100 ppm TEA at 275 °C. However, their sensing response needs further improvement. Recently, our group prepared porous α-Fe_2O_3 nanorods to detect TEA and obtained high response (8.2 for 50 ppm) and fast response time (7 s) at 40 °C [22].

Noble metals like gold and silver decorated on oxide semiconductors can further enhance the sensor sensitivity and selectivity, and also result in higher response as well as lower operating temperature. For instance, Cao et al. [23] synthesized Ag/Cr_2O_3 porous

* Corresponding author at: Materials Research Center for Energy and Photoelectrochemical Conversion, School of Materials Science and Engineering, University of Jinan, Jinan, 250022, Shandong, China.
E-mail address: mse_caobq@ujn.edu.cn (B. Cao).

https://doi.org/10.1016/j.snb.2018.04.096
0925-4005/

microspheres, and their response to 50 ppm of TEA was about 3 times higher than that of pristine Cr_2O_3. Guanwan et al. [24] reported that the response of Au/α-Fe_2O_3 nanorods, which exhibited ultrahigh sensitivity (46.4–100 ppm acetone) at 270 °C. Peeters et al. [25] prepared Au/ε-Fe_2O_3 nanocomposites, which exhibited better selectivity to NO_2 than pure ε-Fe_2O_3 nanocomposites. Zhang et al. [26] developed an efficient, green, and general strategy for the synthesis of Au/α-Fe_2O_3 nanospindles, which also exhibited good sensitivity toward ethanol at 140 °C. Despite the high response obtained, it is inconvenient to fabricate these sensors by the traditional slurry-coating process. Sometimes it may destroy the intrinsic nanostructure physical properties. Thus, the *in-situ* growth of sensing materials on Al_2O_3 electrodes is a promising strategy to simplify the traditional fabrication process.

In this Paper, we report a high-performance Au decahedrons/α-Fe_2O_3 nanorods TEA sensor on flat Al_2O_3 substrate with predesigned electrodes, which can work at near room-temperature. Hematite seed layer are grown on electrodes by a simple sol-gel method. Porous α-Fe_2O_3 NRs directly grow via hydrothermal method and Au DHs are synthesized by one-pot polyol reaction method. Then, Au DHs are decorated onto the porous α-Fe_2O_3 NRs by controlling the spin-coating speed (1000–3000 rpm). Due to the formation of Schottky contact between Au/Fe_2O_3 and the catalytic activity of Au decahedrons, the Au/α-Fe_2O_3 NRs sensor working at 40 °C exhibits higher response and better selectivity to TEA than that of pristine α-Fe_2O_3 NRs sensor. The TEA gas sensing mechanism of Au/α-Fe_2O_3 NRs is discussed in detail.

2. Experimental

2.1. Direct growth of porous α-Fe_2O_3 NRs on flat Al_2O_3 electrodes

The flat Al_2O_3 electrodes (1 mm × 1.5 mm), which consist of a pair of Au electrodes, Pt lead wires, and a heater, were cleaned with ethanol, acetone, and deionized (DI) water by ultrasonication. Hematite seed layer and α-Fe_2O_3 NRs array were *in-situ* grown on flat Al_2O_3 electrodes by sol-gel method and hydrothermal method, respectively. First, 4.054 g ferric chloride ($FeCl_3{\cdot}6H_2O$), 0.211 g polyvinyl alcohol (PVA), and 150 μL hydrochloric acid (HCl 36.5–38%) were dissolved in 50 mL of DI water with continuous stirring to get a clear solution. Hematite seed layers were formed on the cleaned flat Al_2O_3 substrates by spin coating (4000 rpm for 30 s) the above solution, then annealed at 500 °C in air for 2 h. A 30 mL of aqueous solution consisting of 0.810 g $FeCl_3{\cdot}6H_2O$, 2.548 g sodium nitrate ($NaNO_3$), 90 μL HCl, and 160 μL acetontrile was transferred into 50 mL Teflon-lined stainless steel autoclave. At the same time, the flat Al_2O_3 electrodes with seed layer were immersed into the aqueous solution. After the reaction at 100 °C for 4 h, we got the FeOOH NRs. Finally, the precursors were annealed at 650 °C for 20 min in air to obtain the porous α-Fe_2O_3 NRs.

2.2. Growth of Au decahedrons onto porous α-Fe_2O_3 nanorods

On the basis of our experimental design, the growth process of Au DHs/α-Fe_2O_3 NRs arrays is schematically illustrated in Fig. 1. The Au decahedrons were synthesized according to our earlier work [27–29]. Then, the Au DHs-decorated porous α-Fe_2O_3 NRs arrays were grow by spin coating (30 s) a 0.25 mM solution of Au DHs onto the porous α-Fe_2O_3 NRs arrays to form Au/α-Fe_2O_3 heterostructure. By controlling the spin-coating speed (1000, 2000, and 3000 rpm), Au/α-Fe_2O_3 NRs arrays with different loading content of Au DHs were fabricated, and the corresponding gas sensors were named as Au/α-Fe_2O_3 NRs sensor A, B and C, respectively.

2.3. Material characterization and sensor properties testing

The morphology, structure, and crystalline phase of the samples were characterized by field emission scanning electron microscope (FESEM, Quanta FEG250), transmission electron microscope (TEM, JEM-2100F, JEOL), X-ray diffraction (XRD, D8-Advance, Bruker), and X-ray photoelectron spectroscopy (XPS, Thermo ESCALAB 250XI), respectively. The Brunauer-Emmett-Teller (BET) specific surface area of the sample was investigated by measuring nitrogen adsorption–desorption isotherm with a Physisorption Analyzer (Micromeritics Instrument Corporation TriStar II 3020). The corresponding intensity change of the gaseous products including N_2, CO_2, and H_2O was measured by an on line mass spectrometer (MS) (Pfeiffer, MS GSD 320). The gas sensor properties were measured with a static gas-sensing characterization system (WS-60A, Weisheng Electronics, China). The electronic circuit of sensor measurement system is exhibited (Fig. S1), where R_S is the sensor resistance, V_H is the heating voltage, R_L is a loading resistance and the applied voltage (V_c) is 5 V. The desired concentrations of the testing gases is calculated by the following formula:

$$Q = \frac{V \times \varphi \times M}{22.4 \times d \times p} \times 10^{-9} \times \frac{273 + T_R}{273 + T_B} \quad (1)$$

where Q (mL) is the liquid volume of the volatile compound, V (mL) is the volume of the testing chamber, φ is the required gas volume fraction, M (g mol^{-1}) is the molecular weight, d (g cm^{-3}) is the specific gravity, and ρ is the purity of the volatile testing liquid, T_R and T_B (°C) are the temperature at ambient and test chamber, respectively. Firstly, the devices are put into an airproof test box. Test gas such as TEA with calculated concentration is injected into the testing chamber by a microsyringe. Secondly, when the load voltage is not changing, the TEA gas is exposed to the air until the load voltage to the stable again. Finally, the measuring procedure is stopped. The detailed measuring procedures were reported in our earlier work [2,30]. The sensor response (S) was defined as the ratio of R_a/R_g, where R_a and R_g are the resistances of the sensor in air and in target gas, respectively.

3. Results and discussion

3.1. Structural and morphological characteristics

The structure and crystalline phase of the obtained samples were characterized by XRD. Fig. 2 displays the typical XRD spectra of FeOOH, α-Fe_2O_3, and Au/α-Fe_2O_3 NRs samples. All the diffraction peaks of spectrum I can be indexed to FeOOH (JCPDS No. 75–1594) together with XRD peaks from flat Al_2O_3 electrode. After calcination at 650 °C, the sample is identified as hematite (α-Fe_2O_3, JCPDS No. 89-0597). Owing to removal of the OH groups during the calcination process, porous α-Fe_2O_3 NRs are grown [24], as shown in the inset of Fig. 3(a). When the Au DHs are deposited on the α-Fe_2O_3 NRs, the peaks of Au are not detected in spectrum III due to the low loading content.

The morphology of α-Fe_2O_3 and Au/α-Fe_2O_3 NRs was investigated with SEM. As shown in Fig. 3(a), α-Fe_2O_3 NRs grow nearly perpendicular on the substrate and their diameters are about 100 ~ 150 nm with numerous micropores. Fig. 3(b) is the corresponding EDS spectrum of α-Fe_2O_3 NRs. The peaks of O, Fe, and Al can be clearly observed in this spectrum. No other peaks exist for impurities, demonstrating the growth of pure α-Fe_2O_3 NRs on flat Al_2O_3 substrates. Fig. 3(c–h) are the SEM images and the corresponding EDS spectra of α-Fe_2O_3 NRs after Au decorating, indicating that the NRs array morphology can be well maintained. Moreover, the Au content can be well controlled and decreases from 0.25% (Au/α-Fe_2O_3 NRs A) to 0.04% (Au/α-Fe_2O_3 NRs C) as the spin-coating speed increases from 1000 to 3000 rpm.

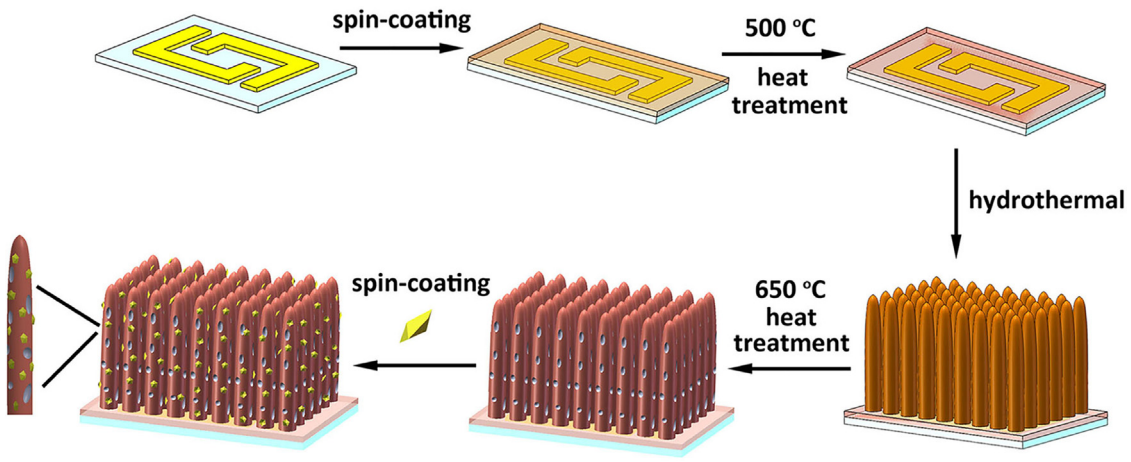

Fig. 1. Schematic for the growth process of Au/α-Fe_2O_3 NRs arrays.

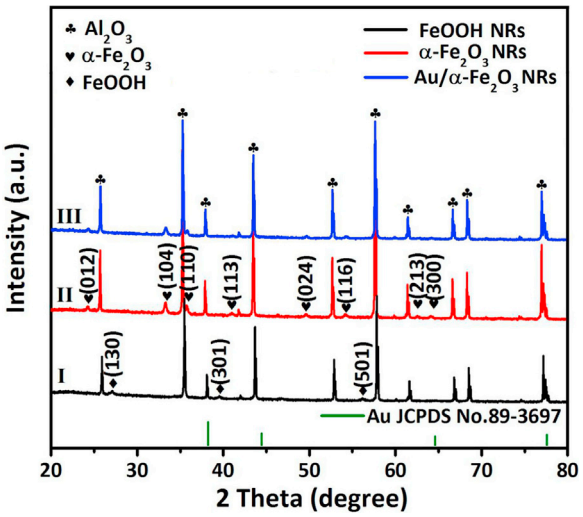

Fig. 2. XRD spectra of the as-synthesized samples on flat Al_2O_3 electrodes. I: FeOOH NRs by hydrothermal method, II: α-Fe_2O_3 NRs by annealing FeOOH NRs, III: α-Fe_2O_3 NRs after Au decorating.

To gain further insights into the microstructures and crystallographic features of the α-Fe_2O_3, Au DHs, and Au/α-Fe_2O_3 NRs, TEM characterizations were employed. Fig. 4(a) depicts the porous structure of pristine α-Fe_2O_3 NRs, which is in good agreement with the SEM observation (the inset of Fig. 3a). Its diameter and length are about 120 nm and 1 μm, respectively. The *d*-spacing between adjacent lattice fringes in the α-Fe_2O_3 NRs is 0.22 nm, which corresponds well to the (113) plane of α-Fe_2O_3 (Fig. 4b). Fig. 4(c) shows the Au DHs with uniform size and the diameter is roughly 30 nm. Fig. 4(d) indicates that the lattice spacing of 0.236 nm in the fringe pattern can be assigned to the Au (111) interplanar distance. Fig. 4(e) and (f) show the TEM and HRTEM images of an Au/α-Fe_2O_3 nanorod. The lattice spacing of 0.25 nm is indexed to the (110) plane of α-Fe_2O_3, while the lattice spacing of 0.236 nm is assigned to the Au (111) plane. It reveals that the Au DHs can be loaded onto α-Fe_2O_3 NRs by the spin-coating to form a typical metal-semiconductor heterojunction.

The surface chemical composition of the as-synthesized Au/α-Fe_2O_3 NRs was further investigated with XPS, as shown in Fig. 5 and Fig. S2/S3. The survey spectrum of Au/α-Fe_2O_3 A in Fig. 5(a) confirms the existence of O, Fe, and Au peaks, besides a relatively weak contribution from adventitious carbon (C 1 s signal at 284.5 eV) due to the atmospheric exposure. To identify all the states of O, Fe, and Au elements, the high resolution spectra of O 1s, Fe 2p, and Au 4f are also measured and shown in Fig. 5(b–d), respectively. The O 1 s spectrum (Fig. 5b) shows three peaks at about 529.8, 531.4, and 532.9 eV, which indicates the presence of three different oxygen species. The peak at 529.8 eV is assigned to the crystal lattice oxygen. The peaks at 531.4 and 532.9 eV correspond to surface adsorbed oxygen and hydroxyl oxygen on the surface, respectively [31]. Fig. 5(c) exhibits two main peaks of Fe $2p_{3/2}$ (710.2 eV) and Fe $2p_{1/2}$ (723.8 eV), with two satellite peaks on their high binding-energy side (at ~8 eV), indicating the Fe^{3+} in iron oxide [32]. Fig. 5(d) presents clear signals for Au $4f_{7/2}$ at 83.5 eV and Au $4f_{5/2}$ at 87.2 eV, which shift to low energy direction in comparison with bulk gold (Au $4f_{7/2}$: 83.8 eV; Au $4f_{5/2}$: 87.5 eV) [33]. This redshift has been reported which is due to the formation of a Schottky junction at Au/α-Fe_2O_3 interface. It also indicates that the electrons in α-Fe_2O_3 transfer to Au DHs [34,35], and more discussion will be presented below. By tuning the spin-coating speed, the Au loading content in Au/α-Fe_2O_3 NR composite is well controlled. The surface atomic content of Au decreases from 18.22%, 2.67% to 0.07% for Au/α-Fe_2O_3 NRs A, B and C. It can be expected that only under optimized loading content the sensor device exhibit better performance (see following discussion).

To investigate the porous structures of the α-Fe_2O_3 NRs, the specific surface area and pore size distribution were calculated from their N_2 adsorption–desorption isotherms, as shown in Fig. 6(b). The porous α-Fe_2O_3 NRs powders are collected by centrifuging the solution after reaction, and the morphology of such porous α-Fe_2O_3 NRs powders (Fig. 6a) is similar to the samples directly grow on the flat Al_2O_3 electrodes. For the porous α-Fe_2O_3 NRs, the Brunauer-Emmett-Teller (BET) specific surface area is measured to be 77.8 $m^2\ g^{-1}$ and the average pore size is mainly distributed at 8 nm (inset of Fig. 6b). The α-Fe_2O_3 NRs samples display a typical type IV adsorption isotherm with a H3-type hysteresis loop at a relative pressure of 0.9-1.0, indicating the presence of the mesoporous structure [36]. Porous materials can greatly accelerate the gas diffusion and provide more effective adsorption sites, which is potentially useful for gas sensor application [37,38].

3.2. Gas sensing property comparison

The gas sensing performances of pristine α-Fe_2O_3 NRs sensor, Au/α-Fe_2O_3 NRs sensor A, B, and C to 50 ppm TEA at 40 °C are shown in Fig. 7(a). The recover resistance is smaller than the initial one. The possible reason is that, after a test reaction in the gas, a certain amount of residual TEA gas may still absorb on the porous α-Fe_2O_3 NRs, which will occupy the effective adsorption sites of oxygen

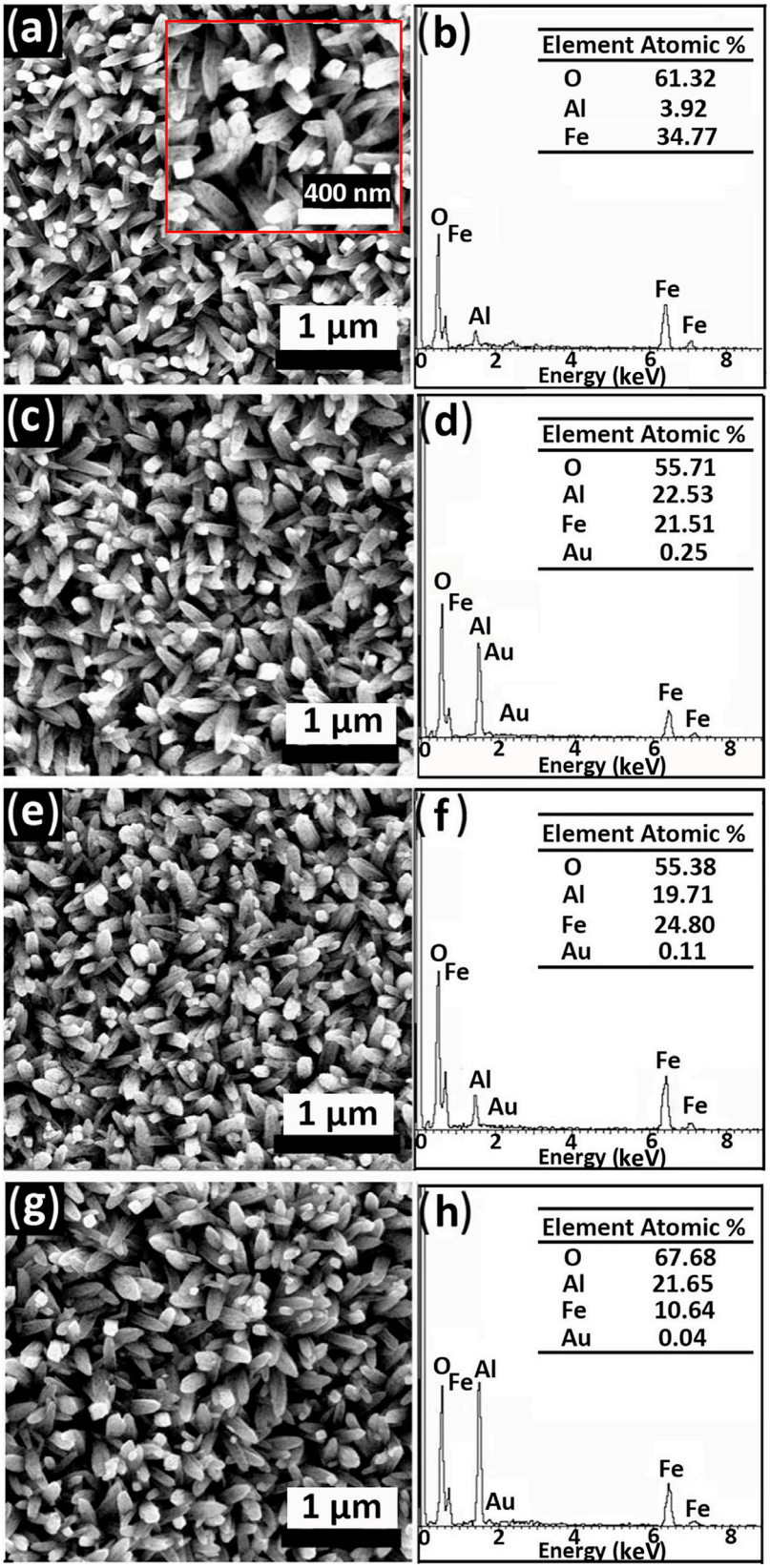

Fig. 3. SEM image of the samples grown in-situ on flat Al_2O_3 electrode and the corresponding EDS spectrum. (a, b) α-Fe_2O_3 NRs; (c-h) Au/α-Fe_2O_3 NRs grown under different spin-coating conditions indicating different gold loading contents.

[39]. In addition, pure Au DHs sensor has no sensing response (Fig. S4). In general, as a typical *n*-type semiconductor gas sensor, when it is exposed to TEA gas, the resistance of the sensor decreases and increases again when it is exposed to air atmosphere [40]. The responses (S = 9.6–17, 40 °C) of Au/α-Fe_2O_3 NRs sensors are all higher than that of α-Fe_2O_3 NRs sensor (S = 9, 40 °C). It reveals that

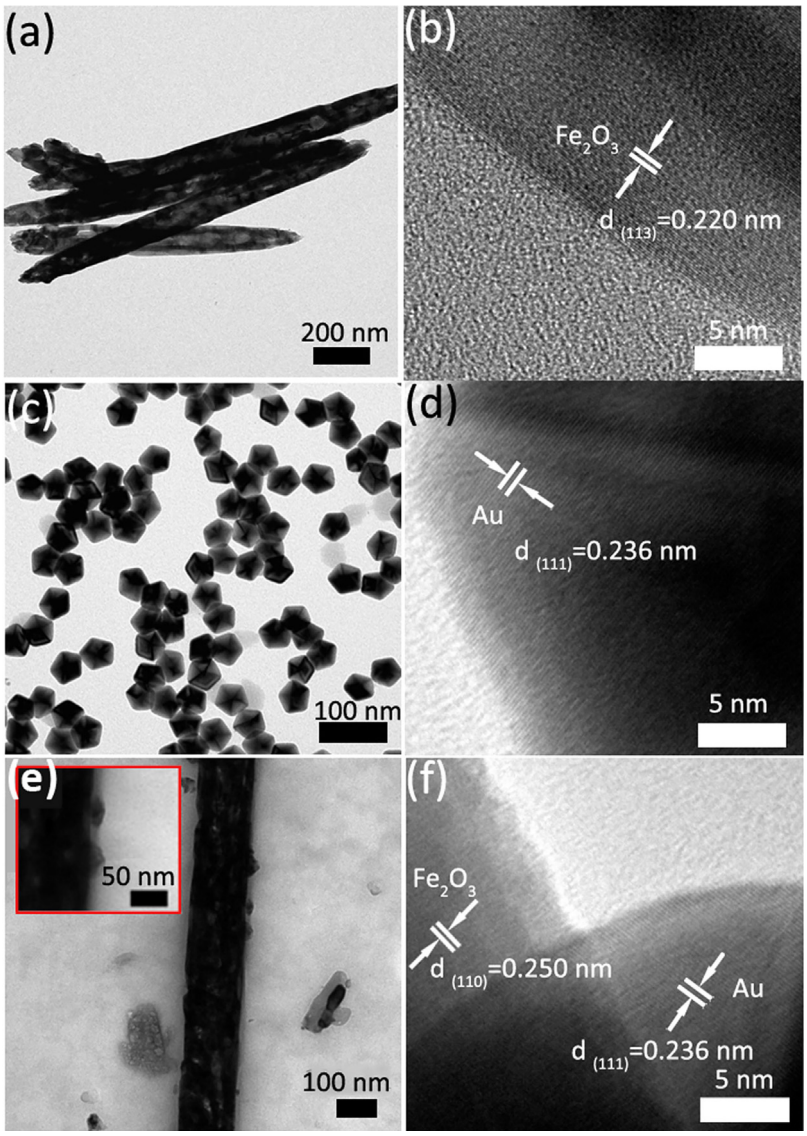

Fig. 4. TEM and HRTEM images. (a, b) pristine α-Fe_2O_3 NRs; (c, d) Au DHs; (e, f) Au/α-Fe_2O_3 NRs.

the sensing performance of α-Fe_2O_3 NRs can be further enhanced by decorating with Au DHs [41]. Moreover, the influence of the Au DHs content on the gas sensing performance is also investigated. All the initial resistances of Au/α-Fe_2O_3 NRs sensors are much higher than that of pure α-Fe_2O_3 NRs sensor due to the formation of open-circuit Schottky junction [42]. As it is very difficult to directly prove the formation of such Schottky junctions between Au nanoparticles and Fe_2O_3 nanowires, we prepared Au/α-Fe_2O_3 film heterostructure to prove the formation of Schottky junction between Au and α-Fe_2O_3 film on fluorine-doped tin oxide (FTO) glass substrates, as shown in Fig. S5(b). Firstly, the α-Fe_2O_3 film was grown by a simple sol-gel method, as adopted for nanowire seed layer growth. Then, Au contact was deposited on the α-Fe_2O_3 film by thermal evaporation. The surface morphology of α-Fe_2O_3 hematite seed layer and Au/α-Fe_2O_3 hematite seed layer was investigated with SEM (the insets of Fig. S5). In addition, Fig. S5(b) also show the EDX atomic percentage of O (65.55%), Fe (16.70%) and Au (17.75%). The corresponding current and voltage (I–V) relationship for different samples (α-Fe_2O_3 film and Au/α-Fe_2O_3) was directly measured with a probe station (Ecopia, EPS300) as shown in the Supporting Information (Fig. S5). The I–V curves of α-Fe_2O_3 film and Au/α-Fe_2O_3 heterostructure exhibit a linear and rectifying characteristic, respectively, proving the Au/α-Fe_2O_3 Schottky contact formation.

The working temperature is one of the most important parameters for gas sensor. Fig. 7(b) shows the response curves of the α-Fe_2O_3 NRs sensor and typical Au/α-Fe_2O_3 NRs sensors toward 50 ppm TEA under different operating temperatures. The highest gas responses are obtained at 180 °C. For example, the maximum response of Au/α-Fe_2O_3 NRs sensor B could as high as 60, while the response of the pristine α-Fe_2O_3 NRs sensor is only 32. Furthermore, the best operating temperature is already much lower than the reported data (~300 °C) for typical MOS sensors [35,43–45]. The sensors can also effectively work at 40 °C with a low heating voltage of 1.24 V. The gas sensor with low power consumption is always highly expected in industrial and home applications. So, the following response curves were all measured at 40 °C to further evaluate their gas sensing properties.

Fig. 8(a) and (b) compare the sensors response and recovery times. Here, the response time (T_{res}) and recovery time (T_{rec}) are defined as the time required for the resistance to reach 90% of the equilibrium value after TEA is introduced, and the time necessary for the sensor to recover 90% of its resistance, respectively [46]. The T_{res} of α-Fe_2O_3 NRs sensor and Au/α-Fe_2O_3 NRs sen-

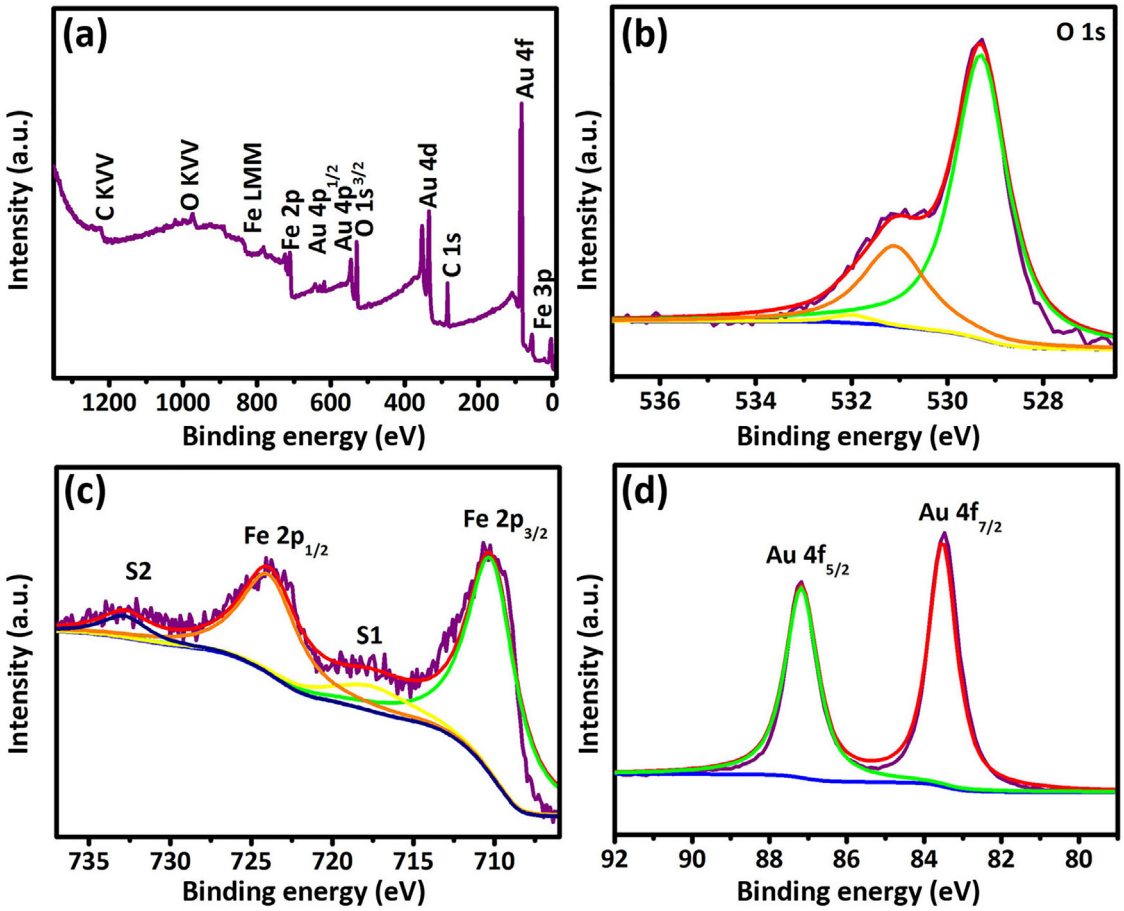

Fig. 5. XPS spectra of the as-synthesized Au/α-Fe_2O_3 NRs A: (a) XPS full survey spectrum; (b) O 1 s spectrum; (c) Fe 2p spectrum; (d) Au 4f spectrum.

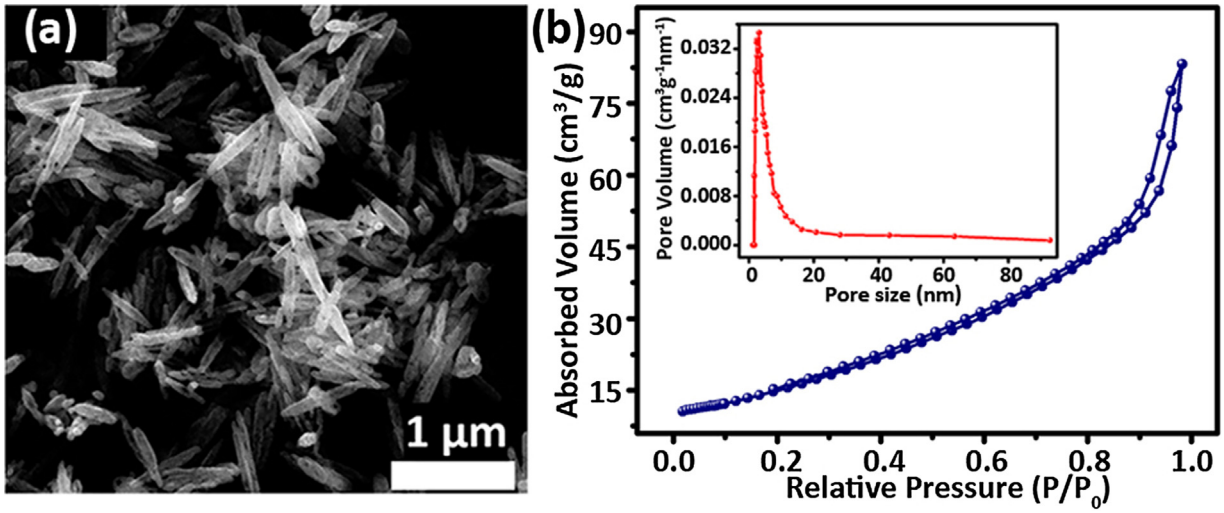

Fig. 6. (a) SEM image of porous α-Fe_2O_3 NRs powders; (b) Typical N_2 adsorption-desorption isotherm and pore size distribution (inset) of porous α-Fe_2O_3 NRs.

sor B toward to 50 ppm of TEA at 40 °C are determined to be 9 s and 12 s, respectively. The response time difference is small. However, the T_{rec} of Au/α-Fe_2O_3 NRs sensor B is 8 s, which is much faster than the pristine α-Fe_2O_3 NRs sensor (T_{rec} = 16 s). Such faster response and recovery time may have two reasons. One reason is the nanoscale porous structure of sensing materials. The size reduction and porous structure can accelerate the gas sensing reaction and thus speed up reaction rate [47]. In addition, the reaction rate is also related to the Schottky contact and the catalytic activity of Au DHs [41].

To further understand the influence of Au modification on the T_{res} and T_{rec}, we also measured the T_{res} and T_{rec} of α-Fe_2O_3 NRs sensor and Au/α-Fe_2O_3 NRs sensor B to various TEA concentration, as shown in Fig. 9. Inset I is the corresponding response time of these two sensors. The response time of Au/α-Fe_2O_3 NRs sensor B to 1, 2, 5, 10, 50, and 100 ppm of TEA is 11, 15, 14, 12, 12, and 11, respectively, whereas the response time of pure α-Fe_2O_3 NRs

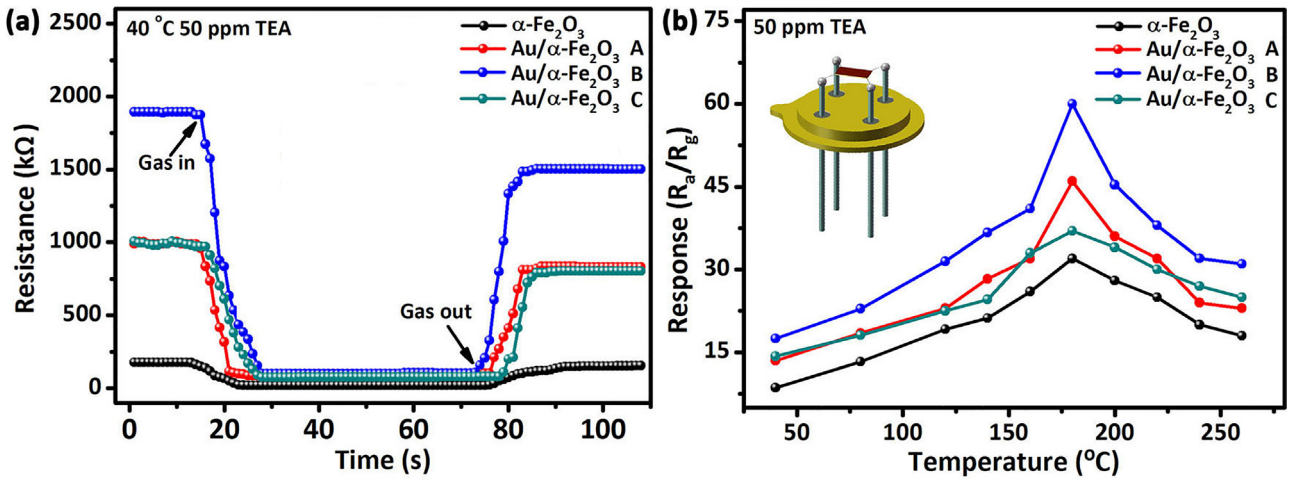

Fig. 7. (a) Resistance curves of pure α-Fe_2O_3 NRs sensor, Au/α-Fe_2O_3 NRs sensors to 50 ppm of TEA at 40 °C; (b) Responses of pure α-Fe_2O_3 NRs sensor and Au/α-Fe_2O_3 NRs sensor (A, B, and C) versus operating temperature to 50 ppm of TEA, (inset pattern) the 3D schematic diagram of the gas sensor.

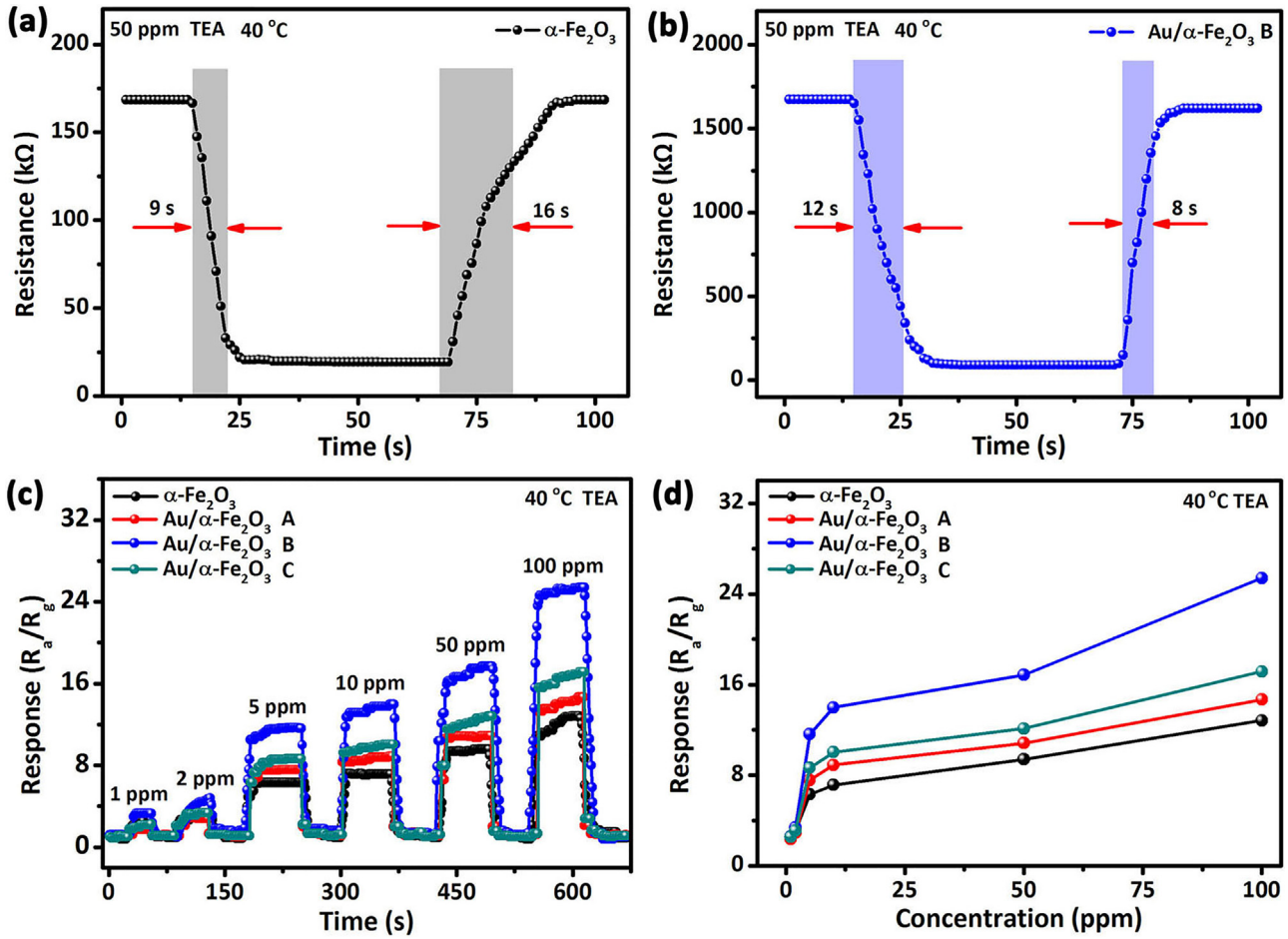

Fig. 8. Response and recovery times of two kinds of sensors: (a) α-Fe_2O_3 NRs sensor; (b) Au/α-Fe_2O_3 NRs sensor B; (c) Response and recovery curves of the four sensors to TEA gas of different concentrations at 40 °C; (d) Corresponding relationship between the sensor response and TEA concentration.

sensor are 18, 17, 16, 13, 9, and 7, respectively. Similarly, inset II is the corresponding recovery time. The recovery time of Au/α-Fe_2O_3 NRs sensor B to 1, 2, 5, 10, 50, and 100 ppm of TEA is 11, 14, 12, 15, 8, and 13, respectively, whereas the recovery time of pure α-Fe_2O_3 NRs sensor is 12, 14, 18, 20, 16, and 15, respectively. Overall, the Au DHs modification speeds up the device recovery.

The response curves of the four α-Fe_2O_3 NRs-based sensors toward TEA of different concentration at 40 °C are depicted in Fig. 8(c). The response of α-Fe_2O_3 NRs-based sensors increases with increasing TEA concentration from 1 to 100 ppm. The Au/α-Fe_2O_3 NRs sensor B exhibits the highest response. Fig. 8(d) shows the corresponding relationship between sensor response and TEA con-

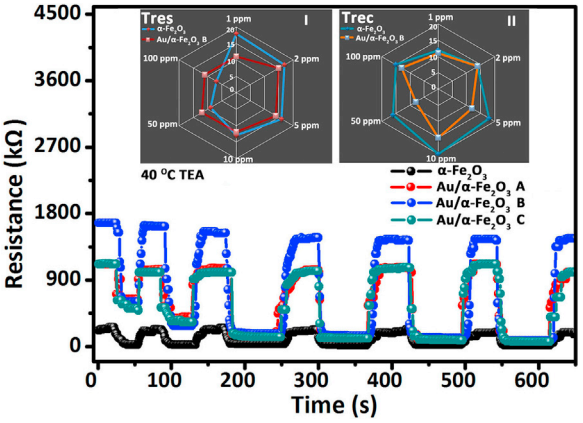

Fig. 9. The response and recovery curve of four sensors to TEA of 1–100 ppm at 40 °C: inset I is the corresponding response time of α-Fe_2O_3 NRs sensor and Au/α-Fe_2O_3 NRs sensor B; inset II is the corresponding recovery time of two kinds of sensors.

centration. For example, the response values of Au/α-Fe_2O_3 NRs sensor B to 1, 2, 5, 10, 50, and 100 ppm of TEA are 2.7, 4, 11.2, 14, 17.5, and 25.4, respectively, whereas the response values of pure α-Fe_2O_3 NRs sensor were 2, 2.5, 6, 7, 8.6, and 12, respectively. Moreover, the Au/α-Fe_2O_3 NRs sensor B shows the better linear characteristic.

To evaluate the repeatability of the four sensors, the successive dynamic response-recovery sensing behavior of five cycles to 50 ppm of TEA has been measured. As shown in Fig. 10(a), the sensor responses exhibit only weak change during the cycling test, indicating their good device repeatability. The sensor stability over 40 days is also checked, as shown in Fig. 10(b). Clearly, the sensors show nearly constant response to 50 ppm of TEA, which illustrates high stability of the gas sensors.

Selectivity is another very important character for gas sensor application [48]. Fig. 10(c) shows the responses of α-Fe_2O_3 NRs sensor and Au/α-Fe_2O_3 NRs sensors to 50 ppm of TEA at 40 °C as well as other gases such as acetone, benzene, *p*-xylene, ethanol, and 2-propanol. The Au/α-Fe_2O_3 NRs sensor B clearly exhibits the highest response towards TEA gas, which is about 5 times higher than that of the response toward other gases, indicating an impressive selectivity toward TEA gas even at low working temperature. The detailed reason for the enhanced selectivity is still not clear now. One possible reason is that the different stability/activity of the target gases. Bond energy is a thermodynamic quantity, and the lower the bond energy, the easier the bond breaks [49]. Here, the bond energies of C—N, C—C, O—H, C=C, C=O are 305, 332, 464, 611, and 728 kJ/mol, respectively [50]. Clearly, the bond strength of C—N in TEA is the weakest. So, TEA is the most unstable one in terms of bond energy among all the target gases in Fig. 10(c). Due to the low C—N bond energy, the high reaction activity of TEA molecules is beneficial to the high response of Au/α-Fe_2O_3 NRs sensors.

The relative humidity (RH) is indeed important for sensor applications. So, we measured the relationship of sensor response and the environment RH at 40 °C, as illustrated in Fig. 10(d). The responses of all sensors decrease with the increasing environment RH. But, when the RH reaches 80%, the responses of the Au/α-Fe_2O_3 NRs sensors are still higher than that of pristine α-Fe_2O_3 NR sensor. In addition, the gas sensing response transients of pure α-Fe_2O_3 NRs sensor and Au/α-Fe_2O_3 NRs sensor B are shown in the Supporting Information (Fig. S6 and Fig. S7). The adsorption of water molecules in high RH environment leads to less chemisorption of oxygen species on the sensing material surface, which leads to the decreasing sensor response in high RH. Moreover, water molecules also act as a barrier against the TEA adsorption. The reactions between the surface oxygen and the water molecules in high RH are conducive to a decrease in the sensor baseline resistance and result in a decrease of the response [22,30].

In general, when an *n*-type oxide semiconductor (Fe_2O_3) is exposed to reducing gas under humid atmosphere, both the water molecule and the reducing gas react with an adsorbed O^{2-} ion. The water molecules (H_2O) react with adsorbed O^{2-} ions on the surface and form the surface hydroxyls (OH^-) prior to the gas sensing reaction, which significantly changes the sensor resistance and deteriorates gas response [51,52]. The reaction between water molecules and adsorbed O^{2-} ions can be described as follows [51].

$$O^{2-}{}_{(ad)} + H_2O_{(M)} \rightarrow 2OH^-{}_{(ad)} \quad (2)$$

However, when the α-Fe_2O_3 nanorod is decorated with moderate Au DHs, Au DHs can serve as specific absorption site to dissociate oxygen molecule (O_2) due to its spillover effect even in wet environment. The O_2 spillover reactions on Au surfaces are presented below [40]:

$$2Au + O_{2(gas)} \rightarrow 2Au/O \quad (3)$$

$$O + e^- \rightarrow O^-{}_{(ads)} \quad (4)$$

Therefore, the Au decahedrons on the Fe_2O_3 surface play a key role in (2) scavenging of hydroxyls (OH^-) on the Fe_2O_3 surface, This mechanism results in the observed humidity independent gas response and sensor resistance.

In conclusion, the sensing properties of the porous α-Fe_2O_3 nanorods sensors have been improved by decorating with Au decahedrons. To highlight the sensor property advantages of our devices, the sensing performance comparisons between our sensors and reported sensors are summarized in Table 1. It is worth noting that the Au/α-Fe_2O_3 nanorod sensor exhibits near room working temperature, lower detection limit, and relatively high response in our work.

3.3. *Gas sensing mechanism of Au/α-Fe_2O_3 nanorods*

The basic gas sensing mechanism of *n*-type MOS such as ZnO, Fe_2O_3, and SnO_2 to reducing gas has been explained with the well-established space charge or depletion layer model [1,21,56]. It depends on the modulation of depletion layer caused by the adsorption and desorption of oxygen molecules [46]. However, when an additional Schottky junction is formed at the metal/semiconductor oxide interface, the sensing mechanism will become different and more complex. Although such improved gas sensing performances are also reported in previous works [2,25,57–59], the detailed sensing mechanism still remains unclearly.

As presented in Fig. 11(a), gold is a typical noble metal with high work function of 5.1 eV [60]. As an *n*-type semiconductor, α-Fe_2O_3 has a band gap energy of 2.1 eV and a work function of 4.39 eV [61]. The contact of noble metal and semiconductor will form a Schottky junction at the interface between the Au decahedron and α-Fe_2O_3 nanorod. As shown in Fig. 11(b), when the α-Fe_2O_3 NR is decorated with Au DHs, the electrons in surface of α-Fe_2O_3 will preferentially transfer to Au, owing to the larger work function of gold compared with that of α-Fe_2O_3. Finally, this results in a charge depletion layer at the Au/α-Fe_2O_3 interface, which further increases the device resistance of the Au/α-Fe_2O_3 NRs sensor than that of pristine α-Fe_2O_3 NRs sensor (Fig. 7a).

The schematic diagram of the gas sensing mechanisms for the Au/α-Fe_2O_3 nanorods is further illustrated in Fig. 11(c and d). As shown in Fig. 11(d), when the pristine α-Fe_2O_3 NR is exposed to air, the oxygen molecules can absorb onto the nanorods surface and capture electrons from α-Fe_2O_3 to form negative oxygen ions $O^{\delta-}$ (O_2^-, O^-, and O^{2-}) [62]. Then an electron surface depletion layer will appear on the surface of α-Fe_2O_3 NR. Moreover, the discrete configuration of Au DHs on the surface of α-Fe_2O_3 NR will

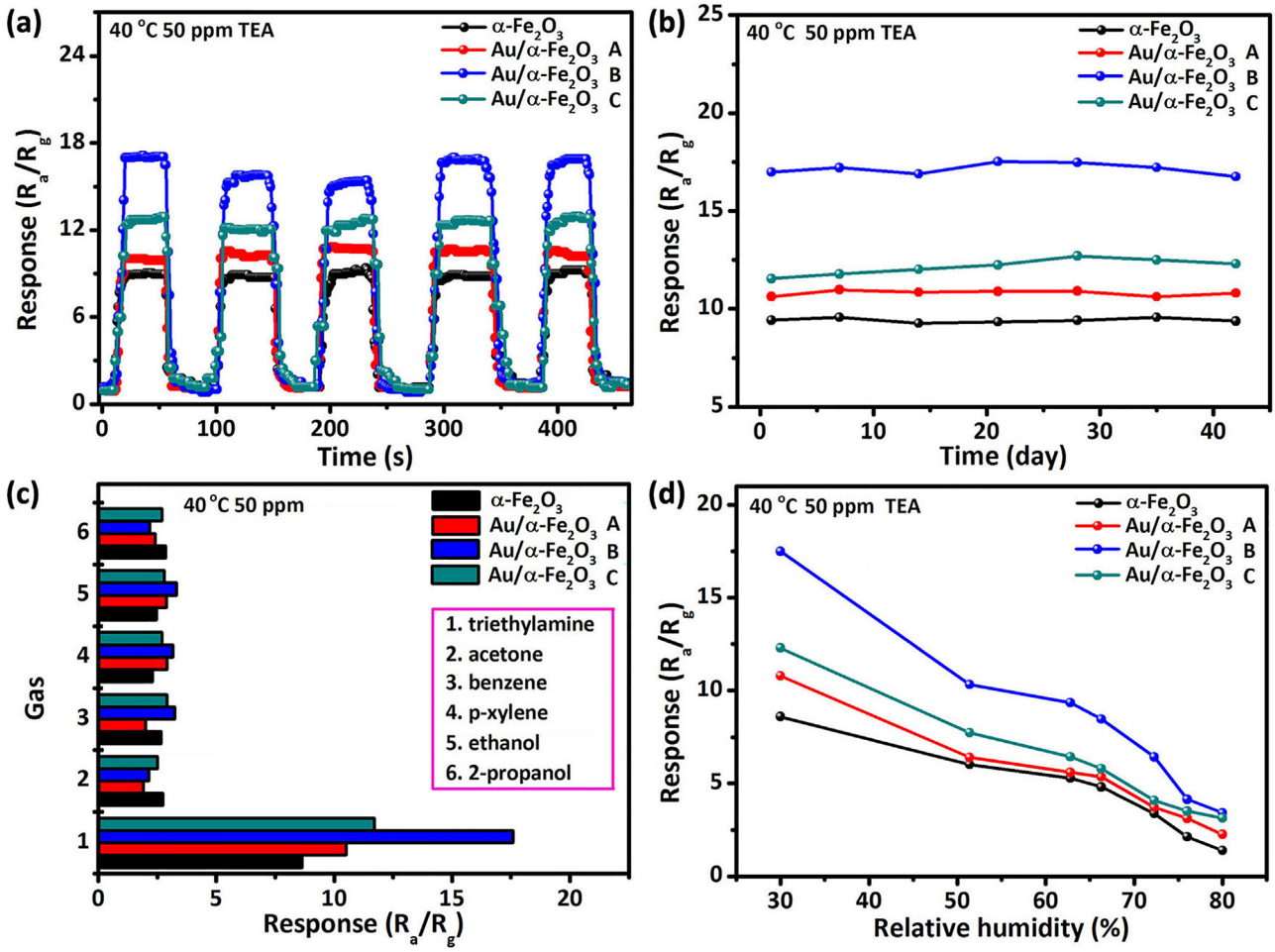

Fig. 10. (a) The device repeatability of pure α-Fe_2O_3 NRs sensor and Au/α-Fe_2O_3 NRs sensors to 50 ppm of TEA at 40 °C; (b) The long term stability measurement of the four sensors to 50 ppm of TEA at 40 °C; (c) The selectivity curves of the four sensors to different target gases at 40 °C; (d) The relationship between the four sensors response and relative humidity.

Table 1
TEA sensing performances of as-prepared sensors in our work and other reported sensors, including concentration (Con.), working temperature (W.T.), sensing resposne (S.R.), response/recovery time (Res./Rec. Time).

Materials	Con. (ppm)	W.T. (°C)	S.R. (R_a/R_g)	Res./Rec. Time (s)	Refs.
SnO_2 hollow microfiber	100	270	49.5	14/12	[1]
ZnO nanorods	50	300	43	10/48	[9]
α-Fe_2O_3 microrod	500	275	41	25/55	[21]
Cr_2O_3 microspheres	50	170	17	29/18	[23]
TiO_2/SnO_2 nanosheets	50	260	25	12/22	[53]
V_2O_5 hollow spheres	100	370	17	40/125	[54]
CuO spheres	100	230	102	21/150	[55]
α-Fe_2O_3 nanorods	50	40	8.6	9/16	Our work
Au/α-Fe_2O_3 nanorods	50	40	17.5	12/8	Our work

further extend the surface depletion layer by forming a Schottky junction [2]. It is worth to note that, when the α-Fe_2O_3 nanorod decorated with excessive Au DHs, the nanorod will be completely covered, and the α-Fe_2O_3 does not participate in the reaction with gas. This may depress the sensor property to reducing TEA [41]. So, the loading amounts of Au DHs should be controlled for better sensor response. In our case, the Au/α-Fe_2O_3 NRs sensor B shows the optimized decorating contents of Au DHs in terms of gas response.

When the Au/α-Fe_2O_3 NR is exposed to the TEA gas, the oxidation-reduction reaction occurs between reducing TEA and $O^{\delta-}$ on Au/α-Fe_2O_3 NR surfaces and the depleted electrons are released back to the conduction region, resulting in a width decrease of the depletion layer and accordingly, the sensor resistance decrease. The reaction between the $O^{\delta-}$ (O_2^-, O^-, and O^{2-}) and TEA molecules can be described as follows [30].

$$2N(C_2H_5)_3 + 39O^-(O_2^-/O^{2-}) = N_2 + 15H_2O + 12CO_2 + 78e^- \quad (5)$$

Three gases (N_2, CO_2, and H_2O) will be produced after the chemical reaction. Experimentally, when 50 ppm TEA gas was injected into the 18 L chamber at 40 °C, the gases were collected immediately. The corresponding mass spectra intensity change of the collected gas before and after chemical reaction was directly measured with an on line mass spectrometer (MS), as shown in Supporting Information (Fig. S8). For the mass spectra, the intensities changes of gas products are analyzed through a preliminary scan from 1 to 50 mass to charge (m/z) value. The signals with m/z

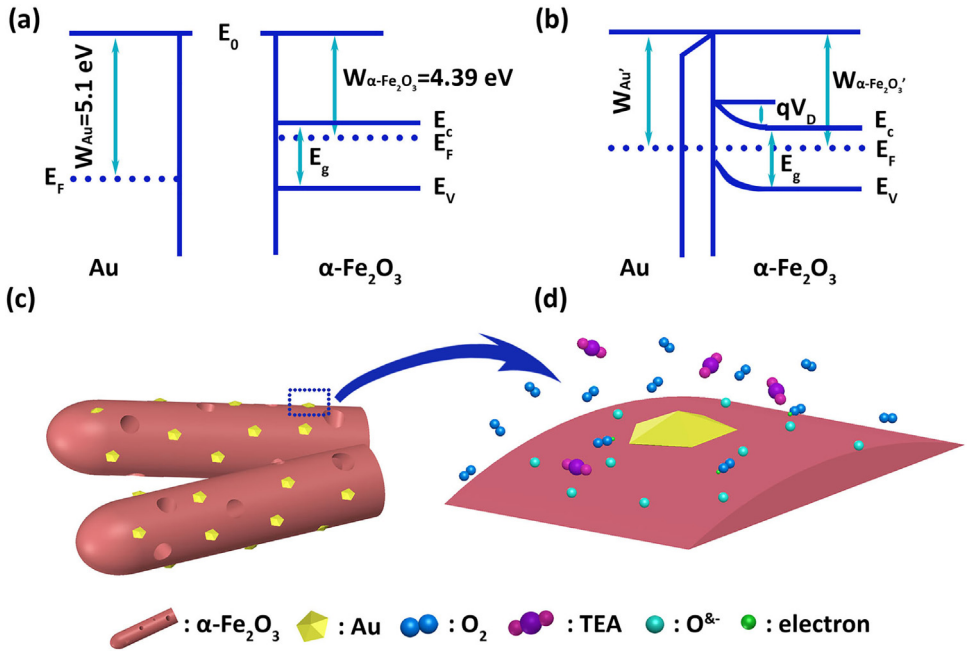

Fig. 11. (a) The energy band diagram of Au DHs and α-Fe_2O_3 NRs; (b) The energy band diagram for a Schottky junction of Au/α-Fe_2O_3 NR with a depletion layer at the surface of α-Fe_2O_3 NR; (c) Diagram of Au/α-Fe_2O_3 nanorods. (d) Schematic model of possible gas mechanisms of the Au/α-Fe_2O_3 nanorods.

ratios of 28, 44, and 18 for N_2, CO_2, and H_2O are shown in Fig. S8(a-c), which shows that the intensities of three kinds of gas increased after the reaction [63].

In addition, another indirect evidence is the resistance change of gas sensor. As shown in Fig. 7(a), when the four kinds of sensors are exposed to the TEA gas, the resistance has obviously decreased, which also indirectly proved that the TEA gas had reacted with the $O^{\delta-}$ at 40 °C. Moreover, the enhanced TEA sensing properties of Au/α-Fe_2O_3 NRs sensor maybe also related to the catalytic of Au DHs [40].

Hence, compared with pristine α-Fe_2O_3 NRs, more absorbed oxygen species will diffuse to the surface of Au/α-Fe_2O_3 NRs at the same time, leading to a lager degree of electrons extractions from the conduction band of α-Fe_2O_3. The high coverage of chemisorbed oxygen species makes the Au/α-Fe_2O_3 NRs more sensitive to TEA gas, which also directly results in a high response. Au is also a common catalyst for the oxidation of reducing gases, which can accelerate the reaction between surface-adsorption oxygen ions species and reducing gases, thus decreasing the recovery time of Au/α-Fe_2O_3 NRs sensor [64].

4. Conclusions

In summary, we design a near room-temperature TEA gas sensor with porous α-Fe_2O_3 nanorods decorated with Au decahedrons and their enhanced gas sensing mechanism is discussed in detail based on the basic principle of M/S Schottky junction. Hematite seed layer directly grow on flat Al_2O_3 electrodes by sol-gel method and porous α-Fe_2O_3 NRs grow *in-situ* on such electrodes by a simple hydrothermal. Then Au DHs with controlled loading content is spun coated onto such α-Fe_2O_3 NRs. The Au/α-Fe_2O_3 NRs sensors exhibit higher and faster response (17–50 ppm), lower detection limit (1 ppm), and better selectivity to TEA even at near room temperature (40 °C) than the pristine α-Fe_2O_3 NR sensor. The enhanced response to TEA is basically attributed to the resistance changes due to the formation of M/S Schottky junction at the Au/α-Fe_2O_3 interface. The catalytic activity of Au DHs may also improve the gas sensing performance of Au/α-Fe_2O_3 NRs. This study provides a rational way for design and fabrication of the chemiresistance gas sensor with high performance.

Acknowledgements

This work is supported by NSFC (11174112) and Shandong Provincial Science Foundation (ZR2017ZB0316).

Appendix A. Supplementary data

Supplementary data associated with this article can be found, in the online version, at https://doi.org/10.1016/j.snb.2018.04.096.

References

[1] Y.H. Zou, S. Chen, J. Sun, J.Q. Liu, Y.K. Che, X.H. Liu, J. Zhang, D.J. Yang, Highly efficient gas sensor using a hollow SnO_2 microfiber for triethylamine detection, ACS Sens. 2 (7) (2017) 897–902.
[2] X.P. Song, Q. Xu, H.Y. Xu, B.Q. Cao, Highly sensitive gold-decorated zinc oxide nanorods sensor for triethylamine working at near room temperature, J. Colloid Interface Sci. 499 (2017) 67–75.
[3] T.M. Cai, L.W. Chen, Q. Ren, S. Cai, J. Zhang, The biodegradation pathway of triethylamine and its biodegradation by immobilized Arthrobacter protophormiae cells, J. Hazard. Mater. 186 (1) (2011) 59–66.
[4] H.Y. Yang, X.L. Cheng, X.F. Zhang, Z.K. Zheng, X.F. Tang, Y.M. Xu, S. Gao, H. Zhao, L.H. Huo, A novel sensor for fast detection of triethylamine based on rutile TiO_2 nanorod arrays, Sens. Actuators B 205 (2014) 322–328.
[5] D.X. Ju, H.Y. Xu, Z.W. Qiu, J. Guo, J. Zhang, Highly sensitive and selective triethylamine-sensing properties of nanosheets directly grown on ceramic tube by forming NiO/ZnO PN heterojunction, Sens. Actuators B 200 (2014) 288–296.
[6] B.Q. Cao, P.A. Smith, C.R.J. Lepage, P.B. Savage, C.R. Bowerbank, E.D. Lee, M.J. Lukacs, Use of a hand-portable gas chromatograph-toroidal ion trap mass spectrometer for self-chemical ionization identification of degradation products related to O-ethyl S-(2-diisopropylaminoethyl) methyl phosphonothiolate (VX), Anal. Chim. Acta 690 (2011) 215–220.
[7] M.A. Lqbal, J.E. Szulejko, K.H. Kim, Determination of methylamine, dimethylamine, and trimethylamine in air by high-performance liquid chromatography with derivatization using 9-fluorenylmethylchloroformate, Anal. Methods 6 (2014) 5697–5707.
[8] J. Zang, X.H. Liu, G. Neri, N. Pinna, Nanostructured materials for room-temperature gas sensors, Adv. Mater. 28 (2016) 795–831.
[9] W.R. Li, H.Y. Xu, T. Zhai, H.Q. Yu, Q. Xu, X.P. Song, J.Q. Wang, B.Q. Cao, High-sensitivity, high-selectivity, and fast-recovery-speed triethylamine sensor based on ZnO micropyramids prepared by molten salt growth method, J. Alloys Compd. 695 (2017) 2930–2936.

[10] R. Li, S. Chen, Z. Lou, L. Li, T.T. Huang, Y.J. Song, D. Chen, G.Z. Shen, Fabrication of porous SnO_2 nanowires gas sensors with enhanced sensitivity, Sens. Actuators B 252 (2017) 79–85.

[11] L. Sun, W.C. Fang, Y. Yang, H. Yu, T.T. Wang, X.T. Dong, G.X. Liu, J.X. Wang, W.S. Yu, K.Y. Shi, Highly active and porous single-crystal In_2O_3 nanosheet for NO_x gas sensor with excellent response at room temperature, RSC Adv. 7 (53) (2017) 33419–33425.

[12] J.M. Ma, L. Mei, Y.J. Chen, Q.H. Li, T.H. Wang, Z. Xu, X.C. Duan, W.J. Zheng, α-Fe_2O_3 nanochains: ammonium acetate-based ionothermal synthesis and ultrasensitive sensors for low-ppm-level H_2S gas, Nanoscale 5 (3) (2013) 895–898.

[13] J.W. Deng, J.M. Ma, L. Mei, Y.J. Tang, Y.J. Chen, T. Lv, Z. Xu, T.H. Wang, Porous α-Fe_2O_3 nanosphere-based H_2S sensor with fast response, high selectivity and enhanced sensitivity, J. Mater. Chem. A 1 (40) (2013) 12400–12403.

[14] S. Yan, G.T. Zan, Q.S. Wu, An ultrahigh-sensitivity and selective sensing material for ethanol: α-/γ-Fe_2O_3 mixed-phase mesoporous nanofibers, Nano Res. 8 (11) (2015) 3673–3686.

[15] H. Pan, L. Jin, B.B. Zhang, H. Su, H.T. Zhang, W.Q. Yang, Self-assembly biomimetic fern leaf-like α-Fe_2O_3 for sensing inflammable 1-butanol gas, Sens. Actuators B 243 (2017) 29–35.

[16] W.X. Jin, S.Y. Ma, Z.Z. Tie, X.H. Jiang, W.Q. Li, J. Luo, X.L. Xu, T.T. Wang, Hydrothermal synthesis of monodisperse porous cube, cake and spheroid-like α -Fe_2O_3 particles and their high gas-sensing properties, Sens. Actuators B 220 (2015) 243–254.

[17] X. Zhou, C. Wang, W. Feng, P. Sun, X.W. Li, G.Y. Lu, Hollow α -Fe_2O_3 quasi-cubic structures: hydrothermal synthesis and gas sensing properties, Mater. Lett. 120 (2014) 5–8.

[18] S. Vallejos, I. Gračia, E. Figueras, C. Cané, Nanoscale heterostructures based on Fe_2O_3@WO_3-x nanoneedles and their direct integration into flexible transducing platforms for toluene sensing, ACS Appl. Mater. Interfaces 7 (2015) 18638–18649.

[19] C.H. Zhao, W.Q. Hu, Z.X. Zhang, J.Y. Zhou, X.J. Pan, E.Q. Xie, Effects of SnO_2 additives on nanostructure and gas-sensing properties of α -Fe_2O_3 nanotubes, Sens. Actuators B 195 (2014) 486–493.

[20] J. Cao, Z.Y. Wang, R. Wang, S. Liu, T. Fei, L.J. Wang, T. Zhang, Synthesis of core–shell α -Fe_2O_3@NiO nanofibers with hollow structures and their enhanced HCHO sensing properties, J. Mater. Chem. A 3 (10) (2015) 5635–5641.

[21] G. Sun, H.L. Chen, Y.W. Li, G.Z. Ma, S.S. Zhang, T.K. Jia, J.L. Cao, X.D. Wang, H. Bala, Z.Y. Zhang, Synthesis and triethylamine sensing properties of mesoporous α -Fe_2O_3 microrods, Mater. Lett. 178 (2016) 213–216.

[22] Q. Xu, Z.C. Zhang, X.P. Song, S. Yuan, Z.W. Qiu, H.Y. Xu, B.Q. Cao, Improving the triethylamine sensing performance based on debye length: a case study on α -Fe_2O_3@NiO (CuO) core-shell nanorods sensor working at near room-temperature, Sens. Actuators B 245 (2017) 375–385.

[23] J. Cao, Y.M. Xu, L.L. Sui, X.F. Zhang, S. Gao, X.L. Chen, H. Zhao, L.H. Huo, Highly selective low-temperature triethylamine sensor based on Ag/Cr_2O_3 mesoporous microspheres, Sens. Actuators B 220 (2015) 910–918.

[24] P. Gunawan, L. Mei, J. Teo, J. Ma, J. Highfield, Q.H. Li, Z.Y. Zhong, Ultrahigh sensitivity of Au/1D α -Fe_2O_3 to acetone and the sensing mechanism, Langmuir 28 (2012) 14090–14099.

[25] D. Peeters, D. Barreca, G. Carraro, E. Comini, A. Gasparotto, C. Maccato, C. Sada, G. Sberveglieri, Au/ε-Fe_2O_3 nanocomposites as selective NO_2 gas sensors, J. Phys. Chem. C 118 (2014) 11813–11819.

[26] J. Zhang, X.H. Liu, L.W. Wang, T.L. Yang, X.Z. Guo, S.H. Wu, S.R. Wang, S.M. Zhang, Au-functionalized hematite hybrid nanospindles: general synthesis, gas sensing and catalytic properties, J. Phys. Chem. C 115 (2011) 5352–5357.

[27] C.C. Li, K.L. Shuford, Q.H. Park, W.P. Cai, Y. Li, E.J. Lee, S.O. Cho, High-yield synthesis of single-crystalline gold nano-octahedra, Angew. Chem. 119 (2007) 3328–3332.

[28] C.C. Li, K.L. Shuford, M.H. Chen, E.J. Lee, S.O. Cho, A facile polyol route to uniform gold octahedra with tailorable size and their optical properties, ACS Nano 9 (2008) 1760–1769.

[29] C.C. Li, L. Sun, Y.Q. Sun, T. Teranishi, One-pot controllable synthesis of Au@Ag heterogeneous nanorods with highly tunable plasmonic absorption, Chem. Mater. 25 (2013) 2580–2590.

[30] Q. Xu, D.X. Ju, Z.C. Zhang, S. Yuan, J. Zhang, H.Y. Xu, B.Q. Cao, Near room-temperature triethylamine sensor constructed with CuO/ZnO PN heterostructural nanorods directly on flat electrode, Sens. Actuators B 225 (2016) 16–23.

[31] L.L. Sui, X.X. Song, X.L. Cheng, X.F. Zhang, Y.M. Xu, S. Gao, P. Wang, H. Zhao, L.H. Huo, An ultraselective and ultrasensitive TEA sensor based on α-MoO_3 hierarchical nanostructures and the sensing mechanism, CrystEngComm 17 (2015) 6493–6503.

[32] R.H. Wang, C.H. Xu, J. Sun, L. Gao, Three-dimensional Fe_2O_3 nanocubes/nitrogen-doped graphene aerogels: nucleation mechanism and lithium storage properties, Sci. Rep. 4 (2014) 7171.

[33] L.H. Zu, Y. Qin, J.H. Yang, In situ synergistic crystallization-induced synthesis of novel Au nanostar-encrusted ZnO mesocrystals with high-quality heterojunctions for high performance gas sensors, J. Mater. Chem. A 3 (2015) 10209–10218.

[34] X.H. Liu, J. Zhang, X.Z. Guo, S.H. Wu, S.R. Wang, Porous α-Fe_2O_3 decorated by Au nanoparticles and their enhanced sensor performance, Nanotechnology 21 (9) (2010) 095501.

[35] X.H. Liu, J. Zhang, X.Z. Guo, S.R. Wang, S.H. Wu, Core–shell α–Fe_2O_3@SnO_2/Au hybrid structures and their enhanced gas sensing properties, RSC Adv. 2 (2012) 1650–1655.

[36] Y.Y. Lü, W.W. Zhan, Y. He, Y.T. Wang, X.J. Kong, Q. Kuang, Z.X. Xie, L.S. Zheng, MOF-templated synthesis of porous Co_3O_4 concave nanocubes with high specific surface area and their gas sensing properties, ACS Appl. Mater. Interfaces 6 (2014) 4186–4195.

[37] T. Wang, Z. Fei, Three-dimensional hierarchical flowerlike α-Fe_2O_3 nanostructures: synthesis and ethanol-sensing properties, ACS Appl. Mater. Interfaces 3 (2011) 4689–4694.

[38] Y.J. Sun, L. Chen, Y. Wang, Z.T. Zhao, P.W. Li, W.D. Zhang, Y.L. Wang, J. Hu, Synthesis of MoO_3/WO_3 composite nanostructures for highly sensitive ethanol and acetone detection, J. Mater. Sci. 52 (2017) 1561–1572.

[39] Q.X. Yu, J.H. Zhu, Z.Y. Xu, X.T. Huang, Facile synthesis of α-Fe_2O_3@SnO_2 core-shell heterostructure nanotubes for high performance gas sensors, Sens. Actuators B 213 (2015) 27–34.

[40] S.M. Majhi, P. Rai, Y.T. Yu, Facile approach to synthesize Au@ZnO core-shell nanoparticles and their application for highly sensitive and selective gas sensors, ACS Appl. Mater. Interfaces 7 (2015) 9462–9468.

[41] G. Korotcenkov, V. Brinzari, B.K. Cho, Conductometric gas sensors based on metal oxides modified with gold nanoparticles: a review, Microchim. Acta 183 (2016) 1033–1054.

[42] W. Tang, J. Wang, Q. Qiao, Z.H. Liu, X.G. Li, Mechanism for acetone sensing property of Pd-loaded SnO_2 nanofibers prepared by electrospinning: fermi-level effects, J. Mater. Sci. 50 (2015) 2605–2615.

[43] X. Han, Y. Sun, Z.Y. Feng, G.C. Zhang, Z.C. Chen, J.H. Zhan, Au-deposited porous single-crystalline ZnO nanoplates for gas sensing detection of total volatile organic compounds, RSC Adv. 63 (2016) 37750–37756.

[44] Y. Li, T. Lv, F.X. Zhao, Q. Wang, X.X. Lian, Y.L. Zou, Enhanced acetone-sensing performance of Au/ZnO hybrids synthesized using a solution combustion method, Electron. Mater. Lett. 11 (2015) 890–895.

[45] W.R. Li, H.Y. Xu, T. Zhai, H.Q. Yu, Z.W. Qiu, X.P. Song, J.Q. Wang, B.Q. Cao, Enhanced triethylamine sensing properties by designing Au@SnO_2/MoS_2 nanostructure directly on alumina tubes, Sens. Actuators B 253 (2017) 97–107.

[46] Y.V. Kaneti, Q.M.D. Zakaria, Z.J. Zhang, C.Y. Chen, J. Yue, M.S. Liu, X.C. Jiang, A.B. Yu, Solvothermal synthesis of ZnO-decorated α-Fe_2O_3 nanorods with highly enhanced gas-sensing performance toward n-butanol, J. Mater. Chem. A 2 (2014) 13283–13292.

[47] Y.J. Chen, C.L. Zhu, L.J. Wang, P. Gao, M.S. Cao, X.L. Shi, Synthesis and enhanced ethanol sensing characteristics of α-Fe_2O_3/SnO_2 core–shell nanorods, Nanotechnology 20 (2008) 045502.

[48] Y.V. Kaneti, J. Moriceau, M. Liu, Y. Yuan, Q. Zakaria, X.C. Jiang, A.B. Yu, Hydrothermal synthesis of ternary α-Fe_2O_3-ZnO-Au nanocomposites with high gas-sensing performance, Sens. Actuators B 209 (2015) 889–897.

[49] L.X. Zhang, J.H. Zhao, H.Q. Lu, L. Li, J.F. Zheng, J. Zhang, H. Li, Z.P. Zhu, Highly sensitive and selective dimethylamine sensors based on hierarchical ZnO architectures composed of nanorods and nanosheet-assembled microspheres, Sens. Actuators B 171 (2012) 1101–1109.

[50] D.X. Ju, H.Y. Xu, Z.W. Qiu, Z.C. Zhang, Q. Xu, J. Zhang, J.Q. Wang, B.Q. Cao, Near room temperature, fast-response, and highly sensitive triethylamine sensor assembled with Au-loaded ZnO/SnO_2 core–shell nanorods on flat alumina substrates, ACS Appl. Mater. Interfaces 7 (2015) 19163–19171.

[51] M. Egashira, M. Nakashima, S. Kawasumi, Temperature programmed desorption study of water adsorbed on metal oxides. 2. Tin oxide surfaces, J. Phys. Chem. 85 (26) (1981) 4125–4130.

[52] J.W. Yoon, J.S. Kim, T.H. Kim, Y.J. Hong, Y.C. Kang, J.H. Lee, A new strategy for humidity independent oxide chemiresistors: dynamic self-Refreshing of In_2O_3 sensing surface assisted by layer-by-layer coated CeO_2 nanoclusters, Small 12 (31) (2016) 4229–4240.

[53] H.Y. Xu, D.X. Ju, W.R. Li, J. Zhang, J.Q. Wang, B.Q. Cao, Superior triethylamine-sensing properties based on TiO_2/SnO_2 n–n heterojunction nanosheets directly grown on ceramic tubes, Sens. Actuators B 228 (2016) 634–642.

[54] M.Z. Wu, X.F. Zhang, S. Gao, X.L. Cheng, Z.M. Rong, Y.M. Xu, H. Zhao, L.H. Huo, Construction of monodisperse vanadium pentoxide hollow spheres via a facile route and triethylamine sensing property, CrystEngComm 15 (46) (2013) 10123–10131.

[55] Y.P. Wu, W. Zhou, W.W. Dong, J. Zhao, X.Q. Qiao, D.F. Hou, D.S. Li, Q.C. Zhang, P.Y. Feng, Temperature-controlled synthesis of porous CuO particles with different morphologies for highly sensitive detection of triethylamine, Cryst. Growth Des. 17 (4) (2017) 2158–2165.

[56] J. Guo, J. Zhang, M. Zhu, D.X. Ju, H.Y. Xu, B.Q. Cao, High-performance gas sensor based on ZnO nanowires functionalized by Au nanoparticles, Sens. Actuators B 199 (2014) 339–345.

[57] S.R. Wang, H.X. Zhang, Y.S. Wang, L.W. Wang, Z. Gong, Facile one-pot synthesis of Au nanoparticles decorated porous α-Fe2O3 nanorods for in situ detection of VOCs, RSC Adv. 4 (2014) 369–373.

[58] T. Goto, T. Itoh, T. Akamatsu, N. Izu, W. Shin, CO sensing properties of Au/SnO_2-Co_3O_4 catalysts on a micro thermoelectric gas sensor, Sens. Actuators B 223 (2016) 774–783.

[59] Z. Zhu, J.L. Chang, R.J. Wu, Fast ozone detection by using a core–shell Au@TiO_2 sensor at room temperature, Sens. Actuators B 214 (2015) 56–62.

[60] Y.F. Bing, Y. Zeng, S.R. Feng, L. Qiao, Y.Z. Wang, W.T. Zheng, Multistep assembly of Au-loaded SnO_2 hollow multilayered nanosheets for high-performance CO detection, Sens. Actuators B 227 (2016) 362–372.

[61] J.Q. Wu, S.Z. Deng, N.S. Xu, J. Chen, Field emission from α-Fe_2O_3 nanoflakes: effect of vacuum pressure, gas adsorption and in-situ thermal treatment, Appl. Surf. Sci. 292 (2014) 454–461.
[62] L. Zhang, Z.L. Liu, L. Jin, B.B. Zhang, H.T. Zhang, M.H. Zhu, W.Q. Yang, Self-assembly gridding (-MoO_3 nanobelts for highly toxic H_2S gas sensors, Sens. Actuators B 237 (2016) 350–357.
[63] G. Özsin, A.E. Pütün, Kinetics and evolved gas analysis for pyrolysis of food processing wastes using TGA/MS/FT-IR, Waste Manag. 64 (2017) 315–326.
[64] X.W. Li, X. Zhou, H. Guo, C. Wang, J.Y. Liu, P. Sun, F.M. Liu, G.Y. Lu, Design of Au@ZnO yolk?shell nanospheres with enhanced gas sensing properties, ACS Appl. Mater. Interfaces 6 (2014) 18661–18667.

Biographies

Xiaopan Song is a graduate student focusing on heterostructure semiconductor gas sensor working at room temperature for master degree at University of Jinan. She was awarded a B.Sc. degree in materials science and engineering from the same university in 2016.

Qi Xu is a graduate student focusing on heterostructure semiconductor gas sensor working at room temperature for master degree at University of Jinan. She was awarded a B.Sc. degree in materials science and engineering from the same university in 2014.

Tao Zhang is a Ph.D student focusing on nanometer catalytic at University of Science and Technology of China. He was awarded a M.S. degree in chemistry and chemical engineering from University of Jinan in 2015.

Bao Song is a graduate student focusing on advanced manufacturing technology and equipment for master degree at University of Jinan. He was awarded a B.Sc. degree in mechanical engineering from the same university in 2016.

Cuncheng Li is a Taishan Scholar Chair Professor for material physics with University of Jinan. He leads a group focusing on new energy, environmental management, chemical/bio-sensing applications of noble metal nanoparticles, inorganic-organic hybrid materials, and metal organic framework materials.

Bingqiang Cao is a Taishan Scholar Chair Professor for material physics with University of Jinan and professor of physics with Qufu Normal University. He leads a group among these two Universities focusing on semiconducting oxide thin films, nanostructures, heterostructures, and related devices.